THE JOURNAL OF PHYSICAL CHEMISTRY B

Article

pubs.acs.org/JPCB

Ultrafast Hydrogen-Bonding Dynamics in the Electronic Excited State of Photoactive Yellow Protein Revealed by Femtosecond Stimulated Raman Spectroscopy

Ryosuke Nakamura,*[,†] Norio Hamada,[†] Kenta Abe,[‡] and Masayuki Yoshizawa[‡]

[†]Science and Technology Entrepreneurship Laboratory, Osaka University, 2-1 Yamada-oka, Suita, Osaka 565-0871, Japan

[‡]Department of Physics, Graduate School of Science, Tohoku University, 6-3 Aramaki-Aza-Aoba, Aoba-ku, Sendai 980-8578, Japan

Supporting Information

ABSTRACT: The ultrafast structural dynamics in the electronic excited state of photoactive yellow protein (PYP) is studied by femtosecond stimulated Raman spectroscopy. Stimulated Raman spectra in the electronic excited state, S_1, can be obtained by using a Raman pump pulse in resonance with the S_1-S_0 transition. This is confirmed by comparing the experimental results with numerical calculations based on the density matrix treatment. We also investigate the hydrogen-bonding network surrounding the wild-type (WT)-PYP chromophore in the ground and excited states by comparing its stimulated Raman spectra with those of the E46Q-PYP mutant. We focus on the relative intensity of the Raman band at 1555 cm^{-1}, which includes both vinyl bond C═C stretching and ring vibrations and is sensitive to the hydrogen-bonding network around the phenolic oxygen of the chromophore. The relative intensity for the WT-PYP decreases after actinic excitation within the 150 fs time resolution and reaches a similar intensity to that for E46Q-PYP. These observations indicate that the WT-PYP hydrogen-bonding network is immediately rearranged in the electronic excited state to form a structure similar to that of E46Q-PYP.

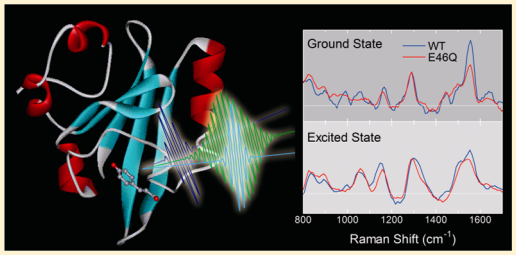

INTRODUCTION

Photoactive yellow protein (PYP) is a 125-residue, 14 kDa photoreceptor protein isolated from *Ectothiorhodospira halophile*.[1] The PYP chromophore consists of a 4-hydroxycinnamic acid covalently bound to Cys69 through a thioester linkage.[2,3] In the ground state, the chromophore is in a deprotonated *trans* form, which is stabilized through a hydrogen-bonding network with Glu46, Tyr42, and Cys69 (Figure 1A).[3] Upon photoexcitation, PYP undergoes a photocycle with a number of intermediate states (Figure 1C), namely, I_0, I_1, and I_2, which involve the *trans*−*cis* isomerization of the chromophore, rearrangement of the hydrogen-bonding network surrounding the chromophore, and large structural changes in the protein.[4−6] PYP returns from the I_2 state to its initial ground state after a few hundred milliseconds.

The initial ultrafast dynamics after photoexcitation have been investigated by various femtosecond spectroscopy techniques. The absorption spectrum of the earliest intermediate state, I_0, which evolves with a time constant of a few picoseconds, is redshifted from the initial ground state.[7] Ultrafast infrared spectroscopy techniques have demonstrated that the *trans*−*cis* isomerization of the chromophore is completed in the I_0 state of PYP.[8−10] The isomerization process is thought to be accompanied by dynamic changes in the hydrogen-bonding network surrounding the chromophore: The hydrogen bond between the chromophore carbonyl group and Cys69 is broken during I_0 state formation, whereas the hydrogen bond between the phenolate group and Glu46 is weakened immediately after photoexcitation and subsequently strengthened during the formation of the I_0 state.[8,9,11]

In E46Q-PYP, glutamic acid is changed to glutamine by using site-directed mutagenesis, as shown in Figure 1B. The E46Q mutation results in a redshift in the ground state absorption maxima and an increase in the rate of recovery from the I_2 state to the initial ground state. On the other hand, similarities in excited state properties for WT-PYP and E46Q-PYP have been reported.[12−15] It has been suggested that the hydrogen bond between Glu46 (Gln46) and the phenolate oxygen of the chromophore in the initial ground state is weaker in the E46Q-PYP mutant than in the wild-type (WT) PYP.[16] X-ray crystallographic studies have also suggested that this is the case.[17,18] A picosecond UV resonance Raman study has shown that this weak hydrogen bond between Gln46 and the phenolate oxygen is similar to the hydrogen bond in the electronic excited state of WT-PYP.[15]

We have performed femtosecond stimulated Raman spectroscopy of WT-PYP and E46Q-PYP to investigate the hydrogen-bonding network participating in the ultrafast photoinduced dynamics of the chromophore in PYP.[19] Ordinary time-resolved Raman spectroscopy has been limited to picosecond time resolution because of the transform limit of the narrow band pulse used for Raman excitation. Femtosecond

Received: August 24, 2012
Revised: November 30, 2012
Published: December 4, 2012

   dx.doi.org/10.1021/jp308433a | J. Phys. Chem. B 2012, 116, 14768−14775

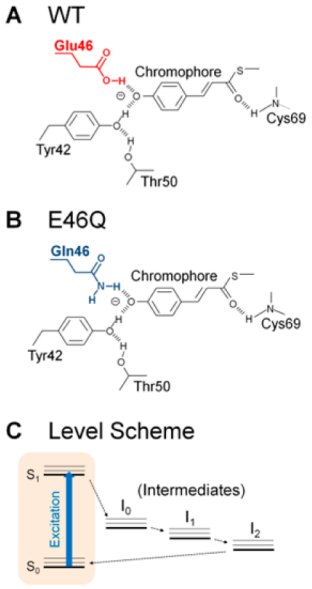

Figure 1. Schematics of the chromophore and the nearby amino acids in the ground states of (A) WT-PYP and (B) E46Q-PYP. (C) Level scheme of PYP showing the initial ground state, S_0, the first excited state, S_1, and a number of the intermediate states.

stimulated Raman spectroscopy has overcome this fundamental limitation and has achieved femtosecond time resolution and spectral resolution of a few tens of wavenumbers. This was accomplished by combining a narrowband Raman pump pulse and an ultrashort probe pulse.[20] In addition, a tunable Raman pump pulse has been developed,[21,22] which is useful for observing a specific transient state by resonant enhancement.

Resonant stimulated Raman scattering in the first excited state S_1 is generally observed by tuning the frequency of the Raman pump pulse to be in resonance with the S_1-S_2 transition, which has an energy of around 27000 cm^{-1} in PYP.[23] In this study, we have performed a stimulated Raman scattering method that exploits the resonance with the S_1-S_0 transition. This method enables us to discuss the stimulated Raman spectra in the S_1 state without knowledge of the S_2 state potential.

Stimulated Raman signals in the S_1 state in resonance with the S_1-S_2 transition have been intensely investigated theoretically and experimentally.[20,24,25] For instance, a spectral shape on the Stokes side is Lorentzian independent of the resonant condition, while that on the anti-Stokes side changes from the Lorentzian to the dispersive shape, depending on the resonant condition. On the other hand, study on stimulated Raman signals in the S_1 state in resonance with the S_1-S_0 transition is limited.[26] Therefore, at first, stimulated Raman spectra were measured on both the Stokes and anti-Stokes sides under various resonant conditions, and they were compared with numerical calculations based on the density matrix treatment to evaluate the physical origin of observed Raman signals.

We confirmed that the observed Raman signal on the anti-Stokes side could be attributed to the Raman process with vibrational coherence in the S_1 state, which was enhanced by resonance with the S_1-S_0 transition. On the other hand, the Raman signal on the Stokes side was attributed to the inverse Raman process with vibrational coherence in the S_1 state.

Next, the anti-Stokes stimulated Raman signals for WT-PYP and E46Q-PYP were compared. We focused on the relative intensities of the Raman band sensitive to the hydrogen bond of the phenolate oxygen. The ultrafast reformation dynamics of the hydrogen bond in the S_1 state were observed upon photoexcitation of WT-PYP, whereas they were not observed for E46Q-PYP.

EXPERIMENTAL METHODS

Sample Preparation. WT-PYP and E46Q-PYP were prepared as previously reported.[27,28] The sample was dissolved in 100 mM Tris-HCl buffer (pH 7.5). The optical density of both samples was 1.0 mm^{-1} at the absorption maximum. The laser spectroscopy measurements were carried out in a 0.5 mm thick flow cell to avoid sample degradation.

Laser Spectroscopy. The femtosecond stimulated Raman spectroscopy setup was based on an amplified mode-locked Ti:Sapphire laser system operating at 1 kHz.[29] A fraction of the amplified pulses was used to drive two independent optical parametric amplifiers (OPA): the femtosecond OPA was pumped by the fundamental pulses (800 nm) and the narrowband OPA was pumped by the second harmonics (400 nm). The femtosecond OPA was used to generate the actinic excitation pulse (460 nm, 100 fs, 80 nJ), which was obtained by the four-wave sum-mixing process ($\omega_{ex} = \omega_p + \omega_i + \omega_i$) in a type I BBO crystal with a fundamental pulse (ω_p) and an idler pulse (ω_i). The narrowband OPA was used to generate the Raman pump pulse. The resonant effect of the stimulated Raman spectrum was studied by using Raman pump pulses with the following center frequencies, full widths at half-maximum (FWHMs), and pulse energies: 19214 cm^{-1}, 32 cm^{-1}, and 80 nJ; 18507 cm^{-1}, 37 cm^{-1}, and 200 nJ; and 17092 cm^{-1}, 31 cm^{-1}, and 400 nJ. In the narrowband OPA, the seed pulse was spectrally filtered before and after amplification by using a spectral filter consisting of a pair of gratings and a slit. The femtosecond supercontinuum generated by a sapphire plate was used as a broadband probe pulse. The fwhm of the cross correlation traces between the actinic excitation and probe pulses was 150 fs. The probe pulse was dispersed onto a linear image sensor with a spectrometer after the overlap of the beams in the sample. The output signals were digitized and collected at the repetition rate of the laser system (1 kHz). The Raman pump beam was modulated at 500 Hz by a mechanical chopper, which was frequency locked to the laser pulse train. The observed spectrum contains Raman features as well as a broad background caused by transient absorption, emission, and other nonlinear effects. We carefully fit the background baseline to a fifth-order polynomial function and then subtracted it from each spectrum. To extract the excited-state Raman spectrum, we subtracted the ground-state Raman spectrum, which was scaled to compensate for a decrease in the ground state population due to actinic excitation. The scaled factor was determined so that the subtraction did not distort the spectral shape. It was confirmed that varying a small amount of the scaled factor did not cause a spectral shift or a change in the relative intensity among the Raman bands but made a spectral shape asymmetric slightly in the case of the anti-Stokes Raman signals.

Numerical Simulation. The spectral features observed in the femtosecond stimulated Raman scattering were investigated by numerically simulating the time evolution of the population and the vibrational coherence with a nonperturbative time-dependent density matrix formalism.[30]

dx.doi.org/10.1021/jp308433a | J. Phys. Chem. B 2012, 116, 14768−14775

First, we consider a multilevel system consisting of vibrational levels in the ground and excited electronic states, $|g_j\rangle$ and $|e_j\rangle$, respectively. The density matrix terms that contribute to our model are $\rho_{gj,gk}$, $\rho_{ej,ek}$, $\rho_{gj,ek}$, and their complex conjugates. The equations for the time evolution of the density matrix affecting the transmittance change of the probe pulse can be written as follows. Note that the electric fields of the probe and Raman pump pulses have different wavevectors: $\mathbf{k}_p$ and $\mathbf{k}_R$. Therefore, we specified the different wavevectors of $\mathbf{k}_p$, $\mathbf{k}_R$, $\mathbf{k}_R$*, and $\mathbf{k}_p + \mathbf{k}_R$* for the density matrix by the additional suffixes p, R, R*, and pR*, respectively.

$$\dot{\rho}_{gj,gk} = (-\gamma_{gj,gk} - i\omega_{gj,gk})\rho_{gj,gk} + \frac{i}{2\hbar}\sum_l (\mu_{el,gk}\rho_{gj,el,R^*}E_R - \mu_{el,gj}\rho_{el,gj,R}E_R^*) \quad (1)$$

$$\dot{\rho}_{gj,gk,pR^*} = (-\gamma_{gj,gk} - i\omega_{gj,gk})\rho_{gj,gk,pR^*} + \frac{i}{2\hbar}\sum_l (\mu_{el,gk}\rho_{gj,el,R^*}E_p - \mu_{el,gj}\rho_{el,gk,p}E_R^*) \quad (2)$$

$$\dot{\rho}_{ej,ek} = (-\gamma_{ej,ek} - i\omega_{ej,ek})\rho_{ej,ek} + \frac{i}{2\hbar}\sum_l (-\mu_{gl,ej}\rho_{gl,ek,R^*}E_R + \mu_{gl,ek}\rho_{ej,gl,R}E_R^*) \quad (3)$$

$$\dot{\rho}_{ej,ek,pR^*} = (-\gamma_{ej,ek} - i\omega_{ej,ek})\rho_{gj,gk,pR^*} + \frac{i}{2\hbar}\sum_l (-\mu_{gl,ej}\rho_{gl,ek,R^*}E_p + \mu_{gl,ek}\rho_{ej,gl,p}E_R^*) \quad (4)$$

$$\dot{\rho}_{ej,gk,p} = (-\gamma_{ej,gk} - i\omega_{ej,gk})\rho_{ej,gk,p} + \frac{i}{2\hbar}\sum_l (-\mu_{gl,ej}\rho_{gj,gk}E_p + \mu_{el,gk}\rho_{ej,el}E_p - \mu_{gl,gk}\rho_{gj,gk,pR^*}E_R + \mu_{el,gk}\rho_{ej,el,pR^*}E_R) \quad (5)$$

$$\dot{\rho}_{ej,gk,R} = (-\gamma_{ej,gk} - i\omega_{ej,gk})\rho_{ej,gk,R} + \frac{i}{2\hbar}\sum_l (-\mu_{gl,ej}\rho_{gj,gk}E_R + \mu_{el,gk}\rho_{ej,el}E_R) \quad (6)$$

The double-sided Feynman diagrams corresponding to the terms in eqs 1−6 are depicted in the Supporting Information. The terms μ, γ, and ω are the dipole coupling coefficient, the dephasing rate, and the energy between the corresponding levels, respectively. This model was numerically solved with a Runge−Kutta algorithm.

The transmittance change, $\Delta T(\omega)/T(\omega)$, of the probe pulse is given by

$$\frac{\Delta T(\omega)}{T(\omega)} \propto -\mathrm{Im}\left\{\frac{\mathbf{F}[\sum \mu_{ej,gk}\rho_{ej,gk,p}]}{\mathbf{F}[E_p(t)]}\right\}$$

where $\mathbf{F}[\cdots]$ represents the Fourier transform. The electric fields of the probe and the Raman pump pulses are expressed as follows:

$$E_p(t) = A_p(t)\ \exp(-i\omega_p t)$$

$$E_R(t) = A_R(t)\ \exp(-i\omega_R t)$$

where $A_p(t)$ and $A_R(t)$ are envelope functions for the probe and Raman pump pulses, respectively.

RESULTS

Stimulated Raman Spectra. Figure 2 shows the stationary absorption and fluorescence spectra of WT-PYP and E46Q-PYP. The absorption and fluorescence peaks were 446 and 492 nm for WT-PYP, respectively. The peaks for E46Q-PYP were 460 and 500 nm, and showed a shift to a longer wavelength compared with WT-PYP. The actinic excitation pulse at 460 nm was in resonance with the S_0−S_1 transition of the chromophore. The three Raman pump pulses used in this study are also plotted in Figure 2.

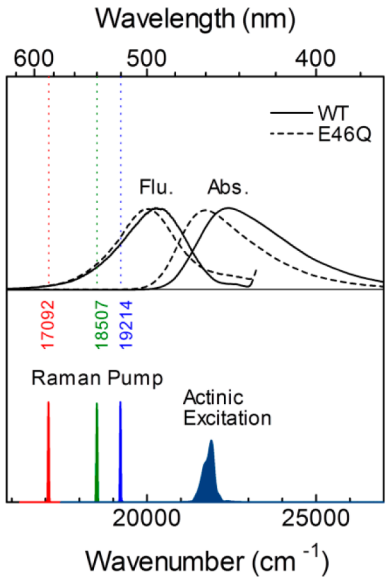

Figure 2. Stationary absorption and fluorescence spectra of WT-PYP (solid line) and E46Q-PYP (broken line). The spectra of the actinic excitation and Raman pump pulses are also shown.

Figure 3A shows the stimulated Raman spectrum on the Stokes side for WT-PYP in the S_0 state, measured without the actinic excitation pulse. The Raman pump energy is 19214 cm^{-1}. The observed Raman spectrum is in agreement with previously reported spontaneous Raman spectra.[31,32] Most of the Raman bands have been assigned based on spontaneous Raman scattering experiments and quantum chemical calculations:[32] the Raman bands in the 1450−1600 cm^{-1} region are related to coupled C−C and C═C stretching modes of the aromatic ring and the ethylenic group; the bands in the 1100−1350 cm^{-1} region are coupled C═C or C−C stretching and in-plane CH rocking modes; and the bands in the region below 1000 cm^{-1} are skeleton or out-of-plane vibrational modes.[32] The intense Raman band at 1555 cm^{-1}, which includes both the vinyl bond C═C stretching and the ring vibrations analogous to Y19a of tyrosine, is sensitive to the hydrogen bond of the phenolate oxygen.[33,34]

The stimulated Raman spectrum on the Stokes side at 0.3 ps after actinic excitation is shown in Figure 3B. The spectrum exhibited a characteristic dispersive spectral shape, which was particularly clear for the Raman bands at 1290 and 1555 cm^{-1}. In contrast, the stimulated Raman spectrum on the anti-Stokes side shown in Figure 3C showed a loss signal with a Lorentzian shape. Note that the vertical axis of Figure 3C indicates Raman loss instead of Raman gain. The peak frequency of each Raman

dx.doi.org/10.1021/jp308433a | J. Phys. Chem. B 2012, 116, 14768−14775

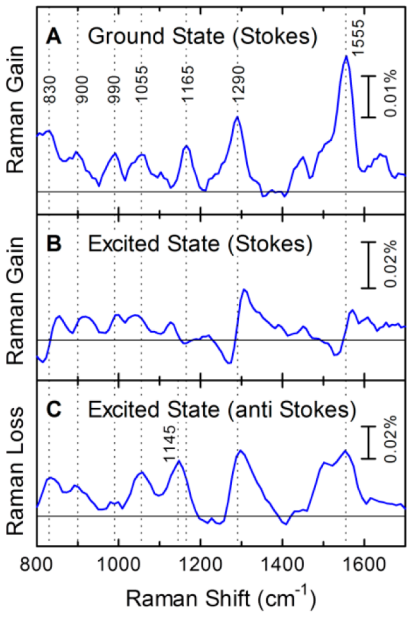

Figure 3. Stimulated Raman spectra of WT-PYP measured with a Raman pump pulse at 19214 cm^{-1}. (A) Raman gain spectrum of the ground state on the Stokes side measured without actinic excitation. (B) Raman gain spectrum of the excited state on the Stokes side measured at 0.3 ps after actinic excitation. (C) Raman loss spectrum of the excited state on the anti-Stokes side measured at 0.3 ps after actinic excitation.

band was similar to that of the ground state, except for the Raman band at 1165 cm^{-1}, which was shifted to 1145 cm^{-1} in the S_1 state. The downshift of the 1165 cm^{-1} mode, which has been assigned to the aromatic ring motion analogous to Y9a of tyrosine, has been also observed by ultrafast infrared spectroscopy.[8,9] A significant difference was also observed in the relative intensity of the Raman signals at 1555 cm^{-1} between the S_0 and S_1 states. The relative intensity in the S_1 state was lower than in the S_0 state.

Figure 4 shows the Raman pump energy dependence of stimulated Raman spectra on the anti-Stokes side at 0.3 ps after actinic excitation. The spectra exhibited a loss signal with a Lorentzian shape with no significant spectral change, although a weak dependence of the relative intensities on the Raman pump energy was observed.

Numerical Simulation Based on the Density Matrix Treatment. The spectral features observed in the stimulated Raman spectroscopy were investigated by numerically simulating the time evolution of the density matrix for two different three-level systems (Figure 5A,D). Because the energy of the Raman pump pulse used in this study was resonant with the S_1-S_0 transition and was much smaller than the S_1-S_2 transition energy, it was sufficient to consider two energy levels for the electronic states. We calculate the time evolution of the density matrix after the excited state population was prepared by actinic excitation. Therefore, the initial condition was set as $\rho_{e0e0} = 1$. For simplicity, $A_p(t)$ and $A_R(t)$ were assumed to be Gaussian functions, and the FWHMs were set so that their Fourier components, $A_p(\omega)$ and $A_R(\omega)$ have FWHMs of 2000 and 20 cm^{-1}, respectively. The center frequency of the probe pulse, ω_p, was set to be the same as ω_R so that the probe pulse width of 2000 cm^{-1} covers both the Stokes and anti-Stokes sides. For the three-level system considered in this study, the dipole coupling coefficients, μ_{jk}, have the same value, μ. The transition rates caused by the external electric fields of $E_p(t)$ and $E_R(t)$ are given by $\mu EP(t)/2\hbar$ and $\mu ER(t)/2\hbar$, respectively. They were determined to be 0.1 ps^{-1} for the probe pulses and 3.0 ps^{-1} for the Raman pulses, which were weak enough not to induce any higher-order effects. The energy, ω_{g0e0}, was set as 20000 cm^{-1}, and the vibrational energy, ω_{g0g1} and ω_{e0e1}, was 1000 cm^{-1}. The dephasing rates of γ_{e0g0}, γ_{g1g0}, and γ_{e1e0}, were 600, 0, and 0 cm^{-1}, respectively. The Raman pump pulse energies used in the calculations were 15000, 18000, and 19000 cm^{-1}. The resonant condition of each pulse energy is slightly different for the two models, resulting in different multiplication factors depicted in Figure 5. For example, in the case of ω_R = 19000 cm^{-1} in Figure 5F, both Raman and probe pulses are perfectly in resonance with the transition energies of ω_{e0g1} and ω_{e0g0}, respectively.

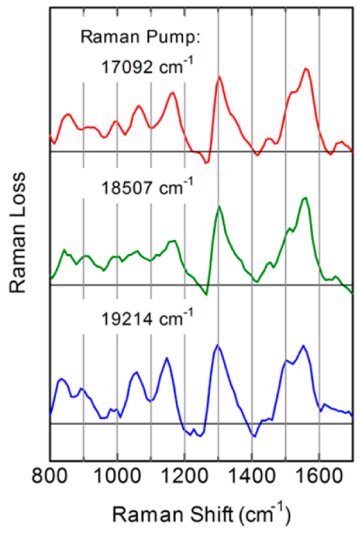

Figure 4. Raman pump energy dependence of stimulated Raman spectra of the excited state on the anti-Stokes side measured at 0.3 ps after actinic excitation.

In the first model, where the vibrational level belonged to the electronic excited state (Figure 5A), the calculated spectra on the Stokes side showed gain signals. The spectral shape changed from the Lorentzian to the dispersive shape as ω_R approached ω_{g0e0}. In contrast, the calculated spectrum on the anti-Stokes side was independent of the resonant condition of the Raman pump pulse. The time evolution of the density matrix for the signal on the Stokes side was $\rho_{e0,e0} \rightarrow \rho_{e0,g0,p} \rightarrow \rho_{e0,e1,pR^*} \rightarrow \rho_{e0,g0,p}$, corresponding to the inverse Raman process, whereas that on the anti-Stokes side was $\rho_{e0,e0} \rightarrow \rho_{g0,e0,R^*} \rightarrow \rho_{e1,e0,pR^*} \rightarrow \rho_{e1,g0,p}$, corresponding to the Raman process.

In the second model, where the vibrational level belonged to the electronic ground state (Figure 5D), the spectral shapes on both sides strongly depended on the resonant condition of the Raman pump pulse; the spectrum changed from a dispersive shape to a loss signal with Lorentzian shape. The time evolution of the density matrix was $\rho_{e0,e0} \rightarrow \rho_{e0,g1,p} \rightarrow \rho_{g0,g1,pR^*} \rightarrow \rho_{e0,g1,p}$ on the Stokes side and $\rho_{e0,e0} \rightarrow \rho_{e0,g0,p} \rightarrow \rho_{g1,g0,pR^*} \rightarrow \rho_{e0,g0,p}$ on the anti-Stokes side. These are vibrationally mediated AC Stark optical processes.[35]

Origin of the Observed Raman Signals. The experimental results indicate that the spectral shape on the Stokes side is dispersive, while that on the anti-Stokes side is a loss signal with a Lorentzian shape independent of the resonant

dx.doi.org/10.1021/jp308433a | J. Phys. Chem. B 2012, 116, 14768−14775

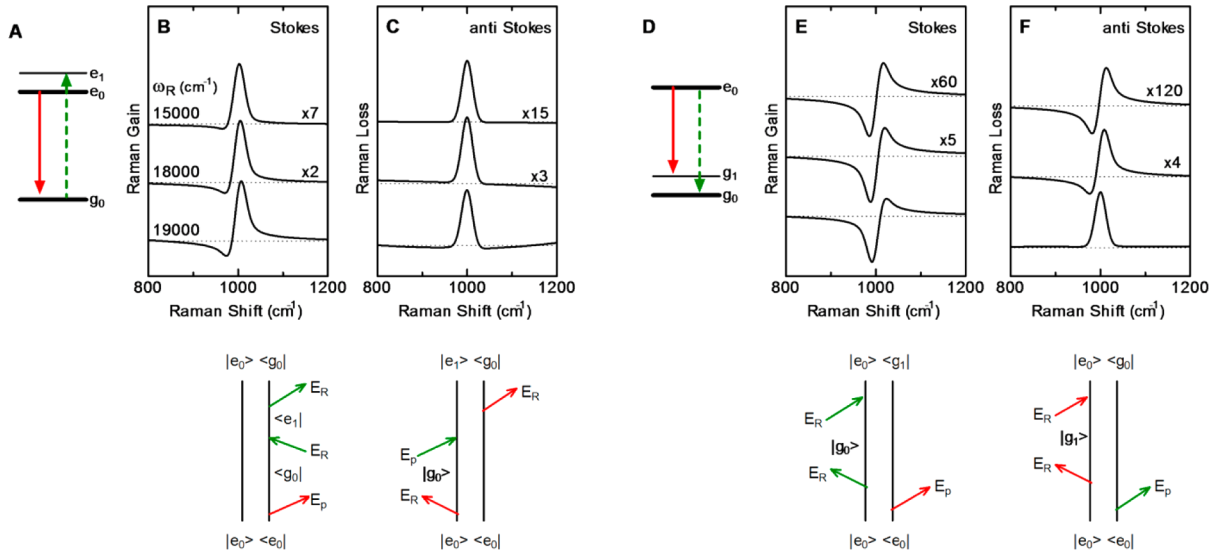

Figure 5. Results of numerical simulations. (A, D) Three-level system used in the simulations. Arrows indicate optical transitions induced by the Raman pump (green broken) and probe (red solid) for the Stokes signal or by the Raman pump (red solid) and probe (green broken) for the anti-Stokes signal. The corresponding double-sided Feynman diagram was depicted in the bottom of each panel. Times run from the bottom to the top. (B) Raman gain spectra on the Stokes side, and (C) Raman loss spectra on the anti-Stokes side calculated, based on the model shown in (A). (E) Raman gain spectra on the Stokes side, and (F) Raman loss spectra on the anti-Stokes side calculated based on the model shown in (D). The center frequencies of the Raman pump pulse, ω_R, are 15000, 18000, and 19000 cm^{-1}.

condition of the Raman pump pulse. These characteristic behaviors of the spectral shapes coincide with the calculated results based on the first model shown in Figure 5A, rather than the second model in Figure 5D. Therefore, we conclude that the transient Raman signals observed on the Stokes and anti-Stokes sides were attributed to the inverse Raman and the Raman processes, respectively, with vibrational coherence in the S_1 state instead of the S_0 state.

Similar dispersive line shapes have been observed in the Stokes spectrum of femtosecond stimulated Raman scattering of bacteriorhodopsin.[36] The resonant condition of the Raman pump pulse in their experiment was similar to the resonant condition in this study; the Raman pump pulse was resonant with the stimulated emission process. The authors postulated that the dispersive shapes were caused by the "Raman initiated by nonlinear emission" (RINE) effect with vibrational coherence in the ground state. However, Niu et al. have performed a simulation based on perturbation theory, which showed that the dispersive line shapes in the Stokes spectrum arose from the inverse Raman scattering with vibrational coherence in the electronic excited state.[26]

In this study, we compared the stimulated Raman spectra on both the Stokes and the anti-Stokes sides with numerical calculations for various resonant conditions. We concluded that the dispersive shape on the Stokes side could be attributed to the inverse Raman scattering with vibrational coherence in the S_1 state, as suggested by Niu et al. On the other hand, the Lorentzian shape on the anti-Stokes side was attributed to Raman scattering with vibrational coherence in the S_1 state.

Comparison of WT-PYP and E46Q-PYP Stimulated Raman Spectra. Figure 6A shows the stimulated Raman spectra on the Stokes side in the S_0 state of WT-PYP and E46Q-PYP. These spectra were normalized to the Raman band at 1290 cm^{-1}. The relative intensity of the Raman band at 1555 cm^{-1} was markedly different, which is consistent with the results reported by Zhou et al.[33]

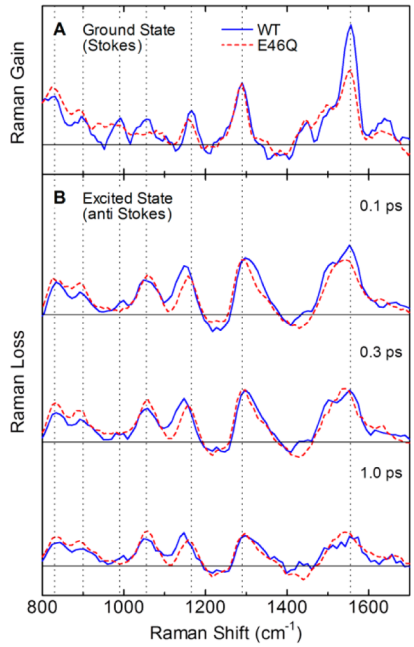

Figure 6. Stimulated Raman spectra of WT-PYP (solid line) and E46Q-PYP (broken line) measured at the ground state, and measured at 0.1, 0.3, and 1.0 ps after actinic excitation. Raman pump energy is 19214 cm^{-1}. (A) Raman gain spectrum of the ground state on the Stokes side. (B) Raman loss spectrum of the excited state on the anti-Stokes side.

Figure 6B shows the femtosecond stimulated Raman spectra on the anti-Stokes side in the S_1 states of WT-PYP and E46Q-PYP at delay times of 0.1, 0.3, and 1.0 ps. The Raman signal from the first intermediate I_0 state was not recognized at a longer delay time because of the insufficient signal-to-noise ratio. As shown in Figure 6, all the Raman modes seem to decrease with time in a uniform way. A remarkable spectral change such as a frequency shift of a Raman band was not

dx.doi.org/10.1021/jp308433a | J. Phys. Chem. B 2012, 116, 14768−14775

observed in the temporal behavior. However, significant spectral features were recognized in a detailed comparison of both samples as follows.

First, the downshift of the 1165 cm^{-1} mode in the S_1 state was only observed for WT-PYP. Next, in contrast to the S_0 state spectra, the relative intensities of the Raman band at 1555 cm^{-1} were the same for WT-PYP and E46Q-PYP. However, the temporal behavior of the relative intensity was slightly different between them. The intensity ratio of the Raman band at 1555 cm^{-1} to that at 1290 cm^{-1}, I_{1555}/I_{1290}, is plotted in Figure 7. In

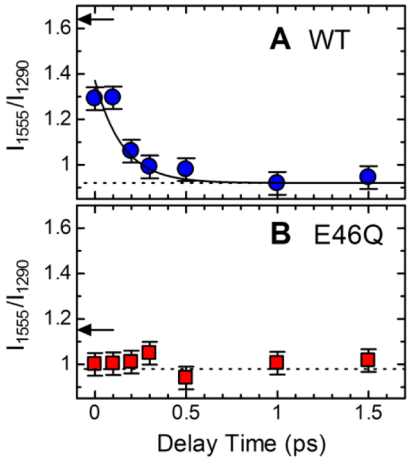

Figure 7. Time profiles of the intensity ratio of the Raman band at 1555 cm^{-1} to that at 1290 cm^{-1}, I_{1555}/I_{1290}, for (A) WT-PYP and (B) E46Q-PYP. Sold line in (A) is an exponential function with a decay time of 150 fs.

the S_0 state, the intensity ratio for WT-PYP was 1.64 (indicated by an arrow in Figure 7A). In the S_1 state, the intensity ratio rapidly decreased and reached a constant value of 0.92. The decay time was comparable with the time resolution of 150 fs. Conversely, the intensity ratio for E46Q-PYP was 0.98, irrespective of the delay time, and was close to an intensity ratio of 1.15 in the S_0 state.

DISCUSSION

The femtosecond stimulated Raman scattering observed on the anti-Stokes side was attributed to the Raman process shown in Figure 5A. Therefore, the vibrational coherence in the S_1 state was coupled to the transition dipole moment of S_1-S_0. The higher excited state did not need to be considered under our experimental conditions, which simplifies the discussion of the relative intensity of the Raman bands.

The relative intensity of the Raman band at 1555 cm^{-1} for WT-PYP immediately decreased in the S_1 state to an intensity similar to that for E46Q-PYP. The following conclusions can be drawn from this observation. (i) In the S_0 state, the hydrogen-bonding network structure around the phenolate oxygen of the chromophore was different for WT-PYP and E46Q-PYP. The vibrational mode at 1555 cm^{-1} was more strongly coupled to the S_0-S_1 transition in WT-PYP than in E46Q-PYP. (ii) Upon actinic excitation of the WT-PYP chromophore, the hydrogen-bonding network immediately rearranged to a structure similar to that in E46Q-PYP within the time resolution of 150 fs. (iii) At the S_1 potential equilibrium, the relative intensity of the Raman band at 1555 cm^{-1} was the same for WT-PYP and E46Q-PYP, and thus had the similar hydrogen-bonding structure.

As for (i), the E46Q mutation is thought to lengthen the distance between the hydrogen atom of Glu (Gln) and the phenolate oxygen of the chromophore in the S_0 state. X-ray crystallography has indicated the difference in the position of the hydrogen atom in WT-PYP and E46 Q in the S_0 state.[17,18] In addition, high-resolution neutron crystallography has been used to analyze the hydrogen positions, and the hydrogen atom in WT-PYP is located almost midway between the carboxyl oxygen and the phenolate oxygen.[37] The localization of the hydrogen atom far from the phenolate oxygen delocalizes the negative charge on the chromophore. It has been suggested that the red shift in the absorption spectrum of E46Q-PYP is a result of the difference in charge distribution.[16]

Experimental[38] and theoretical[39] studies have suggested that a large charge redistribution occurs in the chromophore during the S_0-S_1 transition. In the S_0 state of WT-PYP, the negative charge is localized in the phenolate oxygen, whereas the negative charge is partially delocalized in the S_1 state. Quantum chemical calculations have shown that the large charge redistribution is strongly affected by the nearby Tyr42 and Glu46 amino acids through the hydrogen bonds.[39] Because the vibrational mode at 1555 cm^{-1} is predicted to be strongly coupled to this charge redistribution process, the intensity of the Raman band should also be strongly affected by the hydrogen-bonding network around the phenolate oxygen.

As for (ii), it is considered that the delocalization of the negative charge in the S_1 state of WT-PYP weakens the hydrogen bond with Glu46, which means the hydrogen atom will be nearer to Glu. Consequently, the structure of the hydrogen-bonding network in WT-PYP should resemble that of E46Q-PYP in the S_1 state. The weakening of the hydrogen bond with Glu46 has been observed by ultrafast infrared spectroscopy techniques as an energy shift in the C=O stretch of Glu46.[8,9] In addition, an NMR study of a modified chromophore, which was an analogue of the chromophore in the S_1 state, also suggested that the hydrogen bond with Glu46 was weakened in the S_1 state.[11]

In our observations, the rearrangement of the hydrogen bond in the S_1 state occurred within the time resolution of 150 fs. These ultrafast dynamics are consistent with the ultrafast relaxation from the Franck–Condon state observed by the femtosecond time-resolved fluorescence spectroscopies.[40,41]

As for (iii), similarities in excited state properties for WT-PYP and E46Q-PYP, including fluorescence properties and reaction kinetics, have been pointed out so far.[12−14] These observations suggest that the hydrogen-bonding structure at equilibrium on the S_1 potential of WT-PYP is similar to that of E46Q-PYP. This has also been observed by a UV resonant Raman study of Tyr42 with a picosecond time resolution.[15] Our femtosecond stimulated Raman study of the Raman band, which is sensitive to the structure of the hydrogen bonds, also indicates the same hydrogen-bonding network structure at equilibrium on the S_1 potential.

We also observed the downshift of the 1165 cm^{-1} mode in the S_1 state of WT-PYP. Its temporal behavior after actinic excitation was not clear probably because of the spectral and temporal resolution. In the temporal behavior of the stimulated Raman spectrum in the S_1 state, a remarkable frequency shift was not recognized for the Raman bands in a spectral range of 800−1700 cm^{-1}. In addition to insufficient spectral and temporal resolution, it is considered for a possible reason that the rearrangement of the hydrogen-bonding network around the phenolic oxygen of the chromophore in PYP hardly affects

dx.doi.org/10.1021/jp308433a | J. Phys. Chem. B 2012, 116, 14768−14775

localized vibrational modes located in 800−1700 cm^{-1}. However, it is expected that the 1165 cm^{-1} Raman mode assigned to the aromatic ring motion could be an effective marker band to probe the hydrogen-bonding dynamics around the phenolic oxygen of the chromophore.

CONCLUSIONS

We have compared the stimulated Raman spectra of WT-PYP with those of the E46Q-PYP mutant to investigate the hydrogen-bonding network surrounding the chromophore in the ground and excited states. We focused on the relative intensity of the Raman band at 1555 cm^{-1}, which was sensitive to the hydrogen-bonding network around the phenolic oxygen of the chromophore. The relative intensity of WT-PYP decreased after photoexcitation to that of E46Q-PYP within the time resolution of 150 fs. These observations indicate that the hydrogen-bonding network of WT-PYP was immediately rearranged in the electronic excited state to form a structure similar to that of E46Q-PYP.

ASSOCIATED CONTENT

Supporting Information

Double-sided Feynman diagrams representing time evolution of the density matrix in each term of eqs 1−6. This material is available free of charge via the Internet at http://pubs.acs.org.

AUTHOR INFORMATION

Corresponding Author

*Tel.: +81-6-6879-7755. Fax: +81-6-6879-7755. E-mail: r.nakamura@uic.osaka-u.ac.jp.

Notes

The authors declare no competing financial interest.

ACKNOWLEDGMENTS

This work was supported by JSPS KAKENHI Grant Number 24540323.

REFERENCES

(1) Meyer, T. E. *Biochim. Biophys. Acta* **1985**, *806*, 175−183.
(2) Hoff, W. D.; Düx, P.; Hård, K.; Devreese, B.; Nugteren-Roodzant, I. M.; Crielaard, W.; Boelens, R.; Kaptein, R.; Van Beeumen, J.; Hellingwerf, K. J. *Biochemistry* **1994**, *33*, 13959−13962.
(3) Baca, M.; Borgstahl, G. E. O.; Boissinot, M.; Burke, P. M.; Williams, D. R.; Slater, K. A.; Getzoff, E. D. *Biochemistry* **1994**, *33*, 14369−14377.
(4) Hellingwerf, K. J.; Hendriks, J.; Gensch, T. *J. Phys. Chem. A* **2003**, *107*, 1082−1094.
(5) Ihee, H.; Rajagopal, S.; Srajer, V.; Pah, R.; Anderson, S.; Schmidt, M.; Schotte, F.; Anfinrud, P. A.; Wulff, M.; Keith Moffat, K. *Proc. Natl. Acad. Sci. U.S.A.* **2005**, *102*, 7145−7150.
(6) Bernard, C.; Houben, K.; Derix, N. M.; Marks, D.; van der Horst, M. A.; Hellingwerf, K. J.; Boelens, R.; Kaptein, R.; van Nuland, N. A. J. *Structure* **2005**, *13*, 953−962.
(7) Ujj, L.; Devanathan, S.; Meyer, T. E.; Cusanovich, M. A.; Tollin, G.; Atkinson, G. H. *Biophys. J.* **1998**, *75*, 406−412.
(8) Groot, M. L.; van Wilderen, L. J. G. W.; Larsen, D. S.; van der Horst, M. A.; van Stokkum, I. H. M.; Hellingwerf, K. J.; van Grondelle, R. *Biochemistry* **2003**, *42*, 10054−10059.
(9) Heyne, K.; Mohammed, O. F.; Usman, A.; Dreyer, J.; Nibbering, E. T. J.; Cusanovich, M. A. *J. Am. Chem. Soc.* **2005**, *127*, 18100−18106.
(10) van Wilderen, L. J. G. W.; van der Horst, M. A.; van Stokkum, I. H. M.; Hellingwerf, K. J.; van Grondelle, R. *Proc. Natl. Acad. Sci. U.S.A.* **2006**, *103*, 15050−15055.
(11) Sigala, P. A.; Tsuchida, M. A.; Herschlag, D. *Proc. Natl. Acad. Sci. U.S.A.* **2009**, *106*, 9232−9237.
(12) Philip, A. F.; Nome, R. A.; Papadantonakis, G. A.; Scherer, N. F.; Hoff, W. D. *Proc. Natl. Acad. Sci. U.S.A.* **2010**, *107*, 5821−5826.
(13) Devanathan, S.; Lin, S.; Cusanovich, M. A.; Woodbury, N.; Tollin, G. *Biophys. J.* **2000**, *79*, 2132−2137.
(14) Chosrowjan, H.; Mataga, N.; Shibata, Y.; Imamoto, Y.; Tokunaga, F. *J. Phys. Chem. B* **1998**, *102*, 7695−7698.
(15) Mizuno, M.; Kamikubo, H.; Kataoka, M.; Mizutani, Y. *J. Phys. Chem. B* **2011**, *115*, 9306−9310.
(16) Genick, U. K.; Devanathan, S.; Meyer, T. E.; Canestrelli, I. L.; Williams, E.; Cusanovich, M. A.; Tollin, G.; Getzoff, E. D. *Biochemistry* **1997**, *36*, 8−14.
(17) Anderson, S.; Crosson, S.; Moffat, K. *Acta Crystallogr. D* **2004**, *60*, 1008−1016.
(18) Sugishima, M.; Tanimoto, N.; Soda, K.; Hamada, N.; Tokunaga, F.; Fukuyama, K. *Acta Crystallogr. D* **2004**, *60*, 2305−2309.
(19) (a) Nakamura, R.; Hamada, N.; Kanematsu, Y.; Abe, K.; Yoshizawa, M. Proceedings of The 15th International Conference on Time-Resolved Vibrational Spectroscopy, Ascona, Switzerland, June 19−24, 2011, University of Zurich: Zurich, Switzerland, 2011. (b) Nakamura, R.; Hamada, N.; Kanematsu, Y.; Abe, K.; Yoshizawa, M. Proceedings of The 18th International Conference on Ultrafast Phenomena, Lausanne, Switzerland, July 8−13, 2012, EDP Sciences: France, 2012.
(20) Yoshizawa, M.; Kurosawa, M. *Phys. Rev. A* **1999**, *61*, 013808.
(21) Laimgruber, S.; Schachenmayr, H.; Schmidt, B.; Zinth, W.; Gilch, P. *Appl. Phys. B: Laser Opt.* **2006**, *50*, 557−564.
(22) Shim, S.; Mathies, R. A. *J. Phys. Chem. B* **2008**, *112*, 4826−4832.
(23) Larsen, D. S.; van Stokkum, I. H. M.; Vengris, M.; van der Horst, M. A.; de Weerd, F. L.; Hellingwerf, K. J.; van Gromdelle, R. *Biophys. J.* **2004**, *87*, 1858−1872.
(24) Yoshizawa, M.; Aoki, H.; Hashimoto, H. *Bull. Chem. Soc. Jpn.* **2002**, *75*, 949−955.
(25) Frontinera, R. R.; Shim, S.; Mathies, R. A. *J. Chem. Phys.* **2008**, *129*, 064507.
(26) Niu, K.; Zhao, B.; Sun, Z.; Lee, S. Y. *J. Chem. Phys.* **2010**, *132*, 084510.
(27) Imamoto, Y.; Ito, T.; Kataoka, M.; Tokunaga, F. *FEBS Lett.* **1995**, *374*, 157−160.
(28) Mihara, K.; Hisatomi, O.; Imamoto, Y.; Kataoka, M.; Tokunaga, F. *J. Biochem.* **1997**, *121*, 876−880.
(29) Yoshizawa, M.; Nakamura, R.; Yoshimatsu, O.; Abe, K.; Sakai, S.; Nakagawa, K.; Fujii, R.; Nango, M.; Hashimoto, H. *Acta. Biochim. Polym.* **2012**, *59*, 49−52.
(30) Abe, K. *Ph.D. Thesis*, Tohoku University, Japan, 2012.
(31) Kim, M.; Mathies, R. A.; Hoff, W. D.; Hellingwerf, K. J. *Biochemistry* **1995**, *34*, 12669−12672.
(32) Unno, M.; Kumauchi, M.; Tokunaga, F.; Yamauchi, S. *J. Phys. Chem. B* **2007**, *111*, 2719−2726.
(33) Zhou, Y.; Ujj, L.; Meyer, T. E.; Cusanovich, M. A.; Atkinson, G. H. *J. Phys. Chem. A* **2001**, *105*, 5719−5726.
(34) Devanathan, S.; Brudler, R.; Hessling, B.; Woo, T. T.; Gerwert, K.; Getzoff, E. D.; Cusanovich, M. A.; Tollin, G. *Biochemistry* **1999**, *38*, 13766−13772.
(35) Halle, S. D.; Yoshizawa, M.; Matsuda, H.; Okada, S.; Nakanishi, H.; Kobayashi, T. *J. Opt. Soc. Am. B* **1994**, *11*, 731−736.
(36) McCamant, D. W.; Kukura, P.; Mathies, R. A. *J. Phys. Chem. B* **2005**, *109*, 10449−10457.
(37) Yamaguchi, S.; Kamikubo, H.; Kurihara, K.; Kuroki, R.; Niimura, N.; Shimizu, N.; Yamazaki, Y.; Kataoka, M. *Proc. Natl. Acad. Sci. U.S.A.* **2009**, *106*, 440−444.
(38) Premvardhan, L. L.; van der Horst, M. A.; Hellingwerf, K. J.; van Grondelle, R. *Biophys. J.* **2003**, *84*, 3226−3239.
(39) Gromov, E. V.; Burghardt, I.; Koppel, H.; Cederbaum, L. S. *J. Am. Chem. Soc.* **2007**, *129*, 6798−6806.
(40) Chosrowjan, H.; Mataga, N.; Nakashima, N.; Imamoto, Y.; Tokunaga, F. *Chem. Phys. Lett.* **1997**, *270*, 267−272.

(41) Nakamura, R.; Hamada, N.; Ichida, H.; Tokunaga, F.; Kanematsu, Y. *J. Chem. Phys.* **2007**, *127*, 215102.